**Original Research**

# Diagnostic Performance of MRI Relative to CT for Metastatic Nodes of Head and Neck Squamous Cell Carcinomas

Misa Sumi, DDS, PhD, Yasuo Kimura, DDS, PhD, Tadateru Sumi, DDS, PhD, and Takashi Nakamura, DDS, PhD*

**Purpose:** To compare the diagnostic abilities of magnetic resonance imaging (MRI) and computed tomography (CT) based on the architectural changes in the nodal parenchyma.

**Materials and Methods:** We retrospectively studied histologically proven 70 metastatic and 52 reactive nodes in the necks of 38 patients with head and neck squamous cell carcinomas who had undergone both CT and MRI. We assessed the detectability of the architectural changes in the nodal parenchyma that were suggestive of cancer focus (cancer nest, necrosis, and keratinization). The diagnostic abilities of CT and MRI were assessed by three observers separately for the small (<10 mm in minimum axis diameter) and large (≥10 mm) nodes.

**Results:** MRI was significantly more effective than CT in diagnosing small metastatic nodes, yielding 83% sensitivity, 88% specificity, and 86% accuracy. However, the diagnostic abilities of MRI and CT were similar for large metastatic nodes; MRI yielded 100% sensitivity, 98% specificity, and 99% accuracy. receiver operating characteristic analysis also indicated that the Az values were significantly higher for MRI than for CT (0.927 vs. 0.822, $P = 0.00054$) for the detection of small nodes.

**Conclusion:** MRI is superior to CT in the diagnosis of metastatic nodes from head and neck squamous cell carcinomas.

**Key Words:** MRI; CT; head and neck; lymph node; metastasis
**J. Magn. Reson. Imaging 2007;26:1626–1633.**


THE PRESENCE of metastatic lymph node(s) in the neck significantly reduces the 5-year disease-specific survival in patients with head and neck squamous cell carcinomas (1). Therefore, staging of neck metastasis is a crucial step in managing patients with head and neck squamous cell carcinoma (2). Imaging has greatly contributed to the diagnosis of neck diseases in patients with head and neck cancers. For example, advances in cross-sectional imaging, including helical computed tomography (CT) and magnetic resonance imaging (MRI), have enabled detailed evaluation of both metastatic nodes in the necks and the primary lesions of patients with head and neck carcinomas (3). Compared to conventional CT, the helical CT improved the spatial resolution of the images and could offer information on the nodes, such as nodal size and architectures (4,5). Both nodal size and nodal necrosis have been widely used as criteria for metastatic nodes (6,7). A recent study using the receiver operating characteristic (ROC) curve analysis demonstrated that the performance of CT in detecting metastatic nodes was moderate, with the minimum axis diameter being a better size criterion compared with the maximum axial diameter (8). Nodal necrosis, the other diagnostic criterion, is identified on contrast-enhanced CT as a low-attenuated focal defect with or without enhancement of the nodal periphery (9).

MRI was expected to improve the ability to diagnose metastatic nodes in the neck. However, Curtin et al (10) demonstrated that the performance of MR was equivalent to or less effective than that of CT in the diagnosis of metastatic nodes in the neck. Given the fact that a necrotic focus is identified as a focal defect on contrast-enhanced T1-weighted images as seen on CT, and that MRI was reported to be comparable to CT for the detection of necrosis (9), recent advances in MRI might improve the diagnostic ability of this technique to differentiate between metastatic and reactive nodes in the necks.

In the present study we compared the performance of MRI and CT for the detection of metastatic nodes. We reasoned that the nodal size might influence the diagnostic abilities of MRI and CT; for example, nodal necrosis has been reported to occur in 56% to 63% and 10% to 33% of metastatic nodes larger than 1.5 cm and smaller than 1 cm in maximum axial diameter, respectively (9,11). Furthermore, an important role of the cross-sectional imaging in patient management is the

Department of Radiology and Cancer Biology, Nagasaki University School of Dentistry, Nagasaki, Japan.
*Address reprint requests to: T.N., Professor and Chief, Department of Radiology and Cancer Biology, Nagasaki University School of Dentistry, 1-7-1 Sakamoto, Nagasaki, 852-8588, Japan.
E-mail: taku@nagasaki-u.ac.jp
Received November 20, 2006; accepted August 29, 2007.
DOI 10.1002/jmri.21187
Published online 26 October 2007 in Wiley InterScience (www.interscience.wiley.com).

early detection of nonpalpable metastatic nodes in N0 neck patients. Therefore, we assessed the diagnostic abilities of MRI and helical CT for small (<10 mm in minimum axis diameter) and large (≥10 mm) nodes separately.

## MATERIALS AND METHODS

### *Patients and Lymph Nodes*

The study cohort comprised 38 consecutive patients (6 women and 32 men; average age, 65 years) with head and neck squamous cell carcinoma who had undergone both MR and CT imaging for nodal metastasis in their necks before surgery. We selected the 38 patients from 84 patients with head and neck squamous cell carcinoma who had received surgery for the primary and neck diseases at our hospital from 2003 to 2005. Of the remaining 46 patients, 41 had undergone CT or MRI alone and the 5 were omitted from the present study due to the poor images. There were no patients who had squamous cell carcinoma but had received neither CT nor MRI. Thus, we retrospectively analyzed the MR and CT images of histologically proven metastatic ($n$ = 70) and reactive ($n$ = 52) nodes from the 38 patients for comparing the diagnostic abilities of these two modalities. The primary sites of the patients included the hypopharynx ($n$ = 9), lower gingiva ($n$ = 8), oropharynx ($n$ = 6), upper gingiva ($n$ = 5), tongue ($n$ = 5), oral floor ($n$ = 4), and larynx ($n$ = 1). The metastatic and reactive nodes were divided based on their size (minimum axis diameter) into the small (<10 mm, 34 metastatic and 33 reactive nodes) and large (≥10 mm, 36 metastatic and 19 reactive nodes) groups, as measured on CT images (small nodes : large nodes = 0.94:1 for metastatic nodes, and 1.74:1 for reactive nodes). Twenty of the 38 patients had multiple metastases (2–6 metastatic nodes) in the neck; of these, five patients had multiple metastases on both sides of the neck; 11 patients had a single metastatic node.

### *MRI*

MRI was performed using a 1.5T MR imager (Gyroscan Intera 1.5T Master, Philips Medical System, Best, Netherlands) with a 140 × 170-mm Synergy Flex M, 200-mm Synergy Flex L, or Synergy Head Neck coil (Philips Medical Systems). We obtained T1-weighted (TR/TE/number of signal acquisitions = 500 msec/15 msec/4) and fat-suppressed (spectral presaturation with inversion recovery, SPIR) T2-weighted (TR/TE/number of signal acquisitions = 4677 msec/80 msec/4) axial images of the neck using turbo spin-echo sequences. To compensate for the image intensity inhomogeneity that is inherent to the use of surface coils, we used the CLEAR (constant level appearance) postprocessing technique (Philips Medical Systems). CLEAR uses the premeasured sensitivity profile of the coil to calculate the compensation that is needed to apply on the pixel intensities in order to achieve an even image intensity. We used the parallel imaging technique (SENSE) for fast MRI. The images were obtained using a 200-mm field of view (FOV), 4-mm slice thickness, 0.4 to 0.8-mm slice gap, and a 256 × 204 matrix. For contrast-enhanced studies the patients were intravenously injected with gadolinium at a dose of 0.2 mL/kg body weight.

### *Helical CT*

The patients were scanned using a HiSpeed Advantage SG CT imaging system (General Electric Medical Systems, Milwaukee, WI). Scanning was performed with a 3-mm collimation, 1:1 pitch, a 512 × 512 matrix size, and a 23-cm display FOV at 120 kVp and 160 mA. CT examination was carried out after an intravenous bolus injection of contrast medium (≈100 mL, 2 mL/kg body weight) at a rate of 1.0 mL/sec. We started scanning 80 seconds after the beginning of contrast medium injection. CT scanning for the examination of metastatic nodes in the neck was usually completed within 50–60 seconds after the start of scanning. The scanning period (80–140 seconds after the beginning of contrast medium injection) was confirmed to be the time when the lymph nodes showed plateau-like staining kinetics and provided appropriate contrast against the neighboring muscles. We preferred this rate of contrast medium injection (1.0 mL/sec) instead of faster rates (such as 2.0 mL/sec) because the slower injection rate provided prolonged plateau-like periods for the lymph nodes without any significant loss of enhancement efficiency during the following CT scanning period. We obtained 3-mm thick reformatted axial images from these data.

### *Correlation Between Imaging and Excised Nodes*

We selected the 52 nonmetastatic (reactive) nodes by topographically matching the excised nodes and the CT and MR images using the reporting system that included maps of the necks illustrating approximate locations of the metastatic and reactive nodes relative to the surrounding anatomical structures such as vessels, muscles, salivary glands, and the size of the nodes, as determined on the CT and MR images. At surgery, the nodes were excised en bloc along with the adjacent referring structures and the surgeons correlated the excised nodes with the nodes on the maps. Final decisions regarding the correlations were reached by consensus between the surgeons and radiologists. The excised nodes that matched those on CT and MR images were used for the analysis.

### *Assessment of the Diagnostic Abilities of MRI and CT*

The metastatic and reactive nodes were assessed based on the T1-weighted, fat-suppressed T2-weighted, and contrast-enhanced T1-weighted images. Additionally, they were separately evaluated based on the contrast-enhanced CT. We used the following imaging criteria for metastatic nodes in the neck: A node is diagnosed as metastatic when it displays a nonenhanced area(s) or a weakly enhanced area(s) relative to the surrounding nodal parenchyma (a focal defect indicative of nodal necrosis, or cancer nest, or both) on contrast-enhanced T1-weighted images or contrast-enhanced CT (Figs. 1, 2); on fat-suppressed T2-weighted images, the focal de-

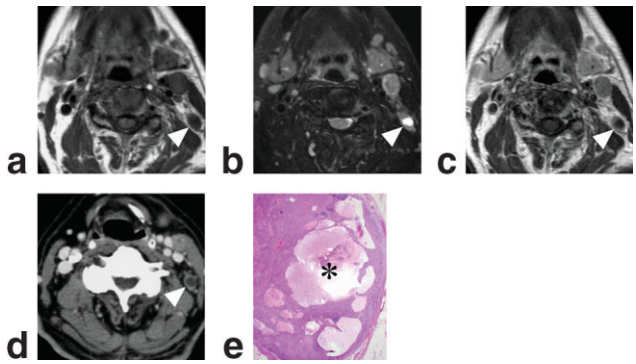


**Figure 1.** A 67-year-old man with carcinoma in the oral floor. **a:** Axial, T1-weighted image (TR/TE = 500 msec/15 msec) shows metastatic node (arrowhead) with hypointense focus at level IIB of the neck. **b:** Axial, fat-suppressed T2-weighted image (TR/TE = 4677 msec/80 msec) shows hyperintense focus in the same metastatic node (arrowhead) as in a. **c:** Axial, contrast-enhanced T1-weighted image (TR/TE = 500 msec/15 msec) show a focal defect in the same metastatic node (arrowhead). **d:** Axial, contrast-enhanced CT shows water-density focal defect in the same metastatic node (arrowhead). **e:** Photomicrograph shows multiple foci of liquefaction necrosis (*) in the same metastatic node. Original magnification ×1. Hematoxylin and eosin staining.

fect may display hyperintense signals (liquefaction necrosis) (Fig. 1b), or hypointense signals (keratin deposits and coagulation necrosis) (Fig. 2b), or both. The necrotic areas are distinct from the nodal hilum, which is hyperintense both on nonenhanced and contrast-enhanced T1-weighted images (Fig. 3a,c), hypointense on fat-suppressed T2-weighted images (Fig. 3b), and shows water to fat density on contrast-enhanced CT (Fig. 3d). Hilar structures are suggestive of reactive nodes (Fig. 3) (12,13). However, when a metastatic focus is still small or is located at the periphery of the node such as the subcapsular to cortical region, the hilum may be still intact and detectable on CT and MR images. In that case, the node may be misdiagnosed as reactive; when a focal defect(s) is seen in a node with hilar structures it is diagnosed as metastatic.

All MR and CT images of the nodes were read in a blinded manner by three radiologists who had 10 to 22 years experience in this field. The blinded reading was performed in an independent fashion among the readers without knowledge of any pathological results. Another radiologist, different from the three observers, had previously rated the quality of the MR and CT images to be used in this study as excellent, good, fair, or poor in terms of the noise of images and motion artifacts. All the images were categorized as excellent or good. Next, the three observers were asked to score whether one or more of the above-mentioned abnormal signals of the nodal parenchyma was present on MR images using a 5-point rating scale (1 = definitely not present, 2 = probably not present, 3 = unclear whether or not the abnormal signal is present or not, 4 = probably present, and 5 = definitely present). At least 2 weeks after the second assessment the observers were again asked to score the presence or absence of the abnormal densities suggestive of cancer foci in the nodal parenchyma on CT images. All lymph nodes that had pathological results were indicated on the images by arrowheads.

We calculated the sensitivity, specificity, and accuracy after placing tentative criteria that probable or definite (= ratings of 4 or 5) presence of abnormal signals in the nodal parenchyma on MR or CT images means nodal metastasis. Negative and positive predictive values were also used to assess the performance of the MRI and CT criteria in the detection of metastatic nodes.

The McNemar test was used to assess the differences in the judgment about the presence or absence of the abnormal signals or densities suggestive of nodal metastasis for MRI or CT among the three observers.

### *ROC Curve Analysis*

We performed ROC curve analysis on the ratings with MRI or CT. For each imaging technique a binormal ROC curve was fitted to each observer's rating data by using ROCKIT software (14). The diagnostic performance of each imaging technique was determined by calculating the area under each observer-specific ROC curve (Az values) (15). Az values were expressed as means ± standard deviations, and the significance of the difference in the Az value between the imaging techniques was tested by the paired *t*-test for each observer.

A two-way analysis of variance (ANOVA) test was performed to assess the differences in the Az values obtained for MRI or CT among the three observers and the two modalities.

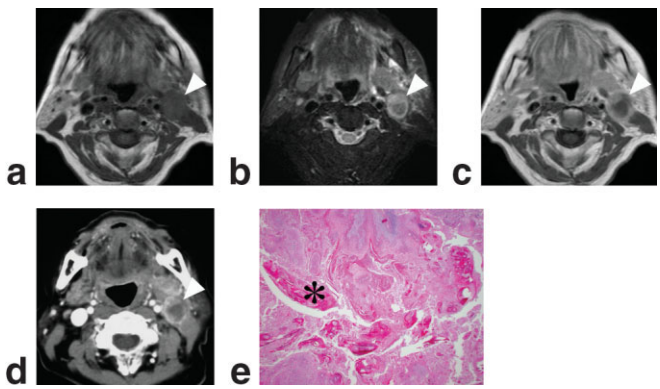


**Figure 2.** A 76-year-old woman with carcinoma in the lower gingiva. **a:** Axial, T1-weighted image (TR/TE = 500 msec/15 msec) shows metastatic node (arrowhead) with homogeneous intensity at level IIA of the neck. **b:** Axial, fat-suppressed T2-weighted image (TR/TE = 4677 msec/80 msec) shows heterogeneously hypointense focus in the same metastatic node as in a. Note honeycomb structures in hypointense focus. **c:** Axial, contrast-enhanced T1-weighted image (TR/TE = 500 msec/15 msec) shows a focal defect in the same metastatic node (arrowhead). **d:** Axial, contrast-enhanced CT shows a focal defect of the same metastatic node (arrowhead) containing high-density structures. **e:** Photomicrograph shows extensive keratin deposits (*) in necrotic focus of the same metastatic node. Original magnification ×1. Hematoxylin and eosin staining.

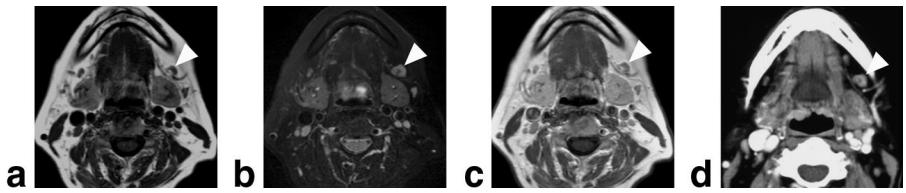


**Figure 3.** A 74-year-old woman with carcinoma in the lower gingiva. **a:** Axial, T1-weighted image (TR/TE = 500 msec/15 msec) shows reactive node (arrowhead) with intact hilar structure at level IB of the neck. Note that hilum is filled with fat tissue signals. **b:** Axial, fat-suppressed T2-weighted image (TR/TE = 4677 msec/80 msec) shows hypointense hilum in the same reactive node (arrowhead) as in a. **c:** Axial, contrast-enhanced T1-weighted image (TR/TE = 500 msec/15 msec) shows homogeneous staining of parenchyma of the same reactive node (arrowhead). Hilum is of fat-intensity signals. **d:** Axial, contrast-enhanced CT shows the same reactive node (arrowhead) with intact hilar structure. Note that hilum exhibits water density.

## RESULTS

MRI provided significantly ($P < 0.05$) higher diagnostic ability to differentiate metastatic nodes from reactive nodes that were smaller than 10 mm in minimum axis diameter in all of the three observers (Figs. 4, 5; Table 1). On averaging the values obtained by the three observers, the MRI yielded 83% sensitivity, 89% specificity, 86% accuracy, and 89% positive and 84% negative predictive values. On the other hand, the CT yielded 68% sensitivity, 79% specificity, 73% accuracy, and 79% positive and 72% negative predictive values. We confirmed that there was no significant difference in the diagnostic ability between the three observers (Table 3), indicating that the higher diagnostic ability of MRI than CT is not due to differences in the diagnostic ability between the observers.

Both MRI and CT provided higher diagnostic performance for nodes that were equal to or greater than 10 mm in minimum axis diameter than for nodes that were smaller than 10 mm in minimum axis diameter (Table 2). In contrast to the small nodes, however, we did not find any significant differences in the diagnostic abilities between the MR and CT imaging for the large nodes. On average, the MRI yielded 100% sensitivity, 98% specificity, 99% accuracy, and 99% positive and 100% negative predictive values. The CT yielded 98% sensitivity, 89% specificity, 95% accuracy, and 95% positive and 97% negative predictive values. Additionally, no significant difference was observed in the diagnostic ability between the observers (Table 3).

The ROC analysis for the small nodes showed that the averaged Az value obtained for MRI (0.925 ± 0.004) was significantly higher than that obtained for CT (0.797 ± 0.030) ($P = 0.0148$, paired $t$-test) (Fig. 6; Table 4). The two-way ANOVA test indicated that a significant difference existed in the Az values between the two modalities ($P = 0.0148$) but not between the observers ($P = 0.3988$).

## DISCUSSION

Here we have shown that in comparison to helical CT, MRI can more readily differentiate metastatic nodes from reactive nodes in the necks of the patients with squamous cell carcinoma. The diagnostic abilities of helical CT and MRI were equivalent with respect to the

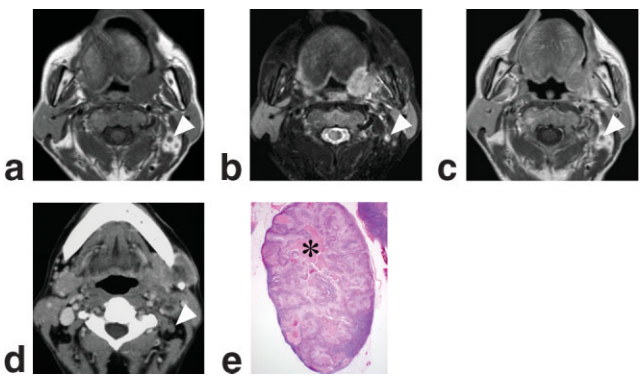


**Figure 4.** A 57-year-old man with carcinoma in the oropharynx. **a:** Axial, T1-weighted image (TR/TE = 500 msec/15 msec) shows small (5 mm in minimum axis diameter) metastatic node (arrowhead) at level IIB of the neck. **b:** Axial, fat-suppressed T2-weighted image (TR/TE = 4677 msec/80 msec) shows hyperintense focus in the same node (arrowhead) as in a. **c:** Axial, contrast-enhanced T1-weighted image (TR/TE = 500 msec/15 msec) shows a focal defect in the same metastatic node (arrowhead). **d:** Axial, contrast-enhanced CT shows the same metastatic node (arrowhead). Note that a small water-density area of this metastatic node is barely distinguishable from hilum on CT. **e:** Photomicrograph of the same metastatic node shows cancer nests associated with necrosis (*). Original magnification ×1. Hematoxylin and eosin staining.

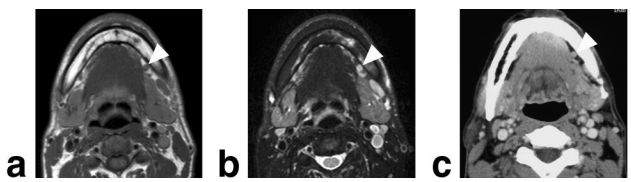


**Figure 5.** A 46-year-old woman with carcinoma in the lower gingival. **a:** Axial, T1-weighted image (TR/TE = 500 msec/15 msec) shows a small (4 mm in minimum axis diameter) reactive node (arrowhead) with intact hilar structure at level IB of the neck. Note small focus filled with fat tissue signals in node. **b:** Axial, fat-suppressed T2-weighted image (TR/TE = 4677 msec/80 msec) shows hypointense focus in the same reactive node (arrowhead) as in a. **c:** Axial, contrast-enhanced CT shows the same reactive node (arrowhead). Note that a small water-density area in this reactive node is barely distinguishable from focal defect on CT. Therefore, a small water-density area of a node on CT as shown in these cases (Figs. 4, 5) may be focal defect indicative of metastatic cancer focus or hilum structure in reactive node. These two distinctive areas are more readily differentiated by MRI.

Table 1
Diagnostic Ability of MR Imaging and Helical CT to Differentiate Metastatic and Reactive Nodes (<10 mm in Minimum Axis Diameter) in the Neck

| | | Diagnostic ability (%) | | |
|---|---|---|---|---|
| | | OB 1 | OB 2 | OB 3 |
| MR vs. CT | McNemar test | MR > CT | MR > CT | MR > CT |
| | *P* value | 0.02535 | 0.04550 | 0.04953 |
| MR | Sensitivity | 82.4 | 85.3 | 82.4 |
| | Specificity | 90.9 | 84.8 | 90.9 |
| | Accuracy | 86.6 | 85.1 | 86.6 |
| | PPV | 90.3 | 85.3 | 90.3 |
| | NPV | 83.3 | 84.8 | 83.3 |
| CT | Sensitivity | 52.9 | 64.7 | 85.3 |
| | Specificity | 90.9 | 84.8 | 60.6 |
| | Accuracy | 71.6 | 74.6 | 73.1 |
| | PPV | 85.7 | 81.5 | 69.0 |
| | NPV | 65.2 | 70.0 | 80.0 |

PPV, positive predictive value; NPV, negative predictive value; OB, observer.

differentiation of large (≥10 mm in maximum axis diameter) nodes. On the other hand, the small (<10mm) nodes were more readily detectable by MRI than by helical CT.

### *Lymph Node Size*

The minimum axis diameter has been a hallmark of metastatic nodes in the neck. The pathological findings of the excised nodes showed that a minimum axis diameter of 10 mm was the most effective size criterion for metastatic nodes in the neck (16). Accumulating evidence has suggested that different size criteria should be used for different levels of the neck; for example, the best criterion may be 1–2 mm greater for the nodes at levels IB and II (16). However, the size criteria of 10 mm or greater may lead to a misdiagnosis of small metastatic nodes as negative for metastasis. This is because a small metastatic focus in a lymph node does not always cause nodal enlargement. In this regard, recent studies on N0-neck patients proposed the best criteria of 8 mm, 9 mm, 6 mm, and 7 mm for metastatic nodes at levels I, II, II, and IV, respectively (7). These studies indicated that it is mandatory to diagnose smaller or nonpalpable nodes for the management of N0 neck patients with squamous cell carcinoma. Therefore, to improve the ability of CT and MRI to diagnose small metastatic nodes, architectural changes of the nodal parenchyma should be carefully considered as the imaging criteria for metastatic nodes.

### *Metastatic Focus*

Metastatic cancer foci contain proliferating cancer cells (cancer nests), necrotic areas, and keratin deposits. Nodal necrosis is considered to be a pathognomonic feature of metastatic nodes from head and neck squamous cell carcinomas. A necrotic focus could be depicted as a focal defect that is not enhanced after an intravenous injection of a contrast medium in CT and MRI (Fig. 1). In most cases the nonenhanced areas (focal defects) are hyperintense on fat-suppressed T2-weighted images, suggesting the presence of liquefaction necrosis. However, some focal defects display low to intermediate signal intensities on fat-suppressed T2-weighted images, indicating the presence of coagulation necrosis or ketatin deposits, or both (17). On the other

Table 2
Diagnostic Ability of MR Imaging and Helical CT to Differentiate Metastatic and Reactive Nodes (≥10 mm in Minimum Axis Diameter) in the Neck

| | | Diagnostic ability (%) | | |
|---|---|---|---|---|
| | | OB 1 | OB 2 | OB 3 |
| MR vs. CT | McNemar test | MR = CT | MR = CT | MR = CT |
| | *P* value | 0.317 | 0.157 | 0.157 |
| MR | Sensitivity | 100.0 | 100.0 | 100.0 |
| | Specificity | 94.7 | 100.0 | 100.0 |
| | Accuracy | 98.2 | 100.0 | 100.0 |
| | PPV | 97.3 | 100.0 | 100.0 |
| | NPV | 100.0 | 100.0 | 100.0 |
| CT | Sensitivity | 100.0 | 100.0 | 94.4 |
| | Specificity | 84.2 | 89.5 | 94.7 |
| | Accuracy | 94.5 | 96.4 | 94.5 |
| | PPV | 92.3 | 94.7 | 97.1 |
| | NPV | 100.0 | 100.0 | 90.0 |

PPV, positive predictive value; NPV, negative predictive value; OB, observer.

Table 3
Assessment of Differences in Diagnostic Ability Between Observers

| | McNemar test (*P* value) | |
|---|---|---|
| | MR | CT |
| Small nodes (<10 mm minimum axis diameter) | | |
| OB 1 vs. OB 2 | 0.763 | 0.527 |
| OB 2 vs. OB 3 | 0.782 | 0.808 |
| OB 1 vs. OB 3 | 0.739 | 0.670 |
| Large nodes (≥10 mm minimum axis diameter) | | |
| OB 1 vs. OB 2 | 0.317 | 0.317 |
| OB 2 vs. OB 3 | 1.000 | 0.564 |
| OB 1 vs. OB 3 | 0.317 | 1.000 |

OB, observer.

hand, these two types of necrosis cannot be readily differentiated on CT images.

Nodal necrosis has been reported to occur in 56% to 63% and 10% to 33% of metastatic nodes larger than 1.5 cm and smaller than 1 cm in maximum axial diameter, respectively (9,11). Another study showed that 35% of metastatic nodes associated with nodal necrosis were smaller than 1 cm in minimum axis diameter (7). Nodal necrosis occurs as cancer cells infiltrate into the medullary portion of the nodes and surpass the available blood supply. Therefore, nodal necrosis can occur even in a small metastatic node with a small metastatic focus (Fig. 4). On contrast-enhanced CT images, it may often be difficult to differentiate between the nodal necrosis (water density) (Fig. 4) and the intact hilar structure (water to fat density) (Figs. 3, 5) in small metastatic nodes. Even in such cases, contrast-enhanced T1-weighted imaging could differentiate between nodal necrosis and hilar structures. In addition, the characteristically hyperintense signals from the necrotic areas on fat-suppressed T2-weighted images would be very suggestive of metastatic nodes (Fig. 4). These distinctive

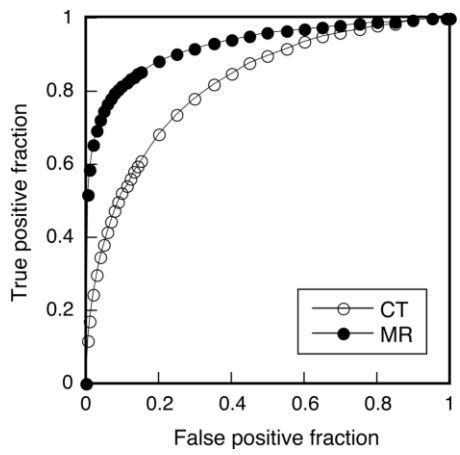


**Figure 6.** Graph shows averaged ROC curves created from the averaged ROC curve parameters of each of the three observers for small (<10 mm in minimum axis diameter) nodes by abnormal findings in nodal parenchyma that are suggestive of cancer foci. Note that MRI performs better than CT does.

Table 4
ROC Analysis for Diagnostic Performance of MR Imaging and Helical CT in Differentiating Between Metastatic and Reactive Nodes (<10 mm in Minimum Axis Diameter)

| | Az values | | |
|---|---|---|---|
| | OB 1 | OB 2 | OB 3 |
| MR | 0.9210 | 0.9257 | 0.9292 |
| CT | 0.7636 | 0.8223 | 0.8062 |

Az values = areas under the receiver operator characteristic (ROC) curves. OB, observer.

findings by MRI may explain its higher performance than CT in differentiating small metastatic from reactive nodes (Table 1; Figs. 4, 5). In contrast, the abnormal signals in the nodal parenchyma, which were derived from necrosis, cancer nests, or keratinization, were easily detectable in large metastatic nodes. Thus, the diagnostic abilities of CT and MRI appeared to be at a similar level in large nodes (Table 2).

Keratinization is another pathognomonic feature of metastatic nodes from well-differentiated types of head and neck squamous cell carcinomas (16). Keratin deposits are depicted by nonenhanced CT as high-density areas or spots in the metastatic cancer foci; enhanced CT may obliterate keratin deposits in cancer foci. On the other hand, the keratin deposits could be recognized as low-intensity areas or spots on contrast-enhanced T1-weighted and fat-suppressed T2-weighted images.

We did not use fat suppression in the contrast-enhanced MRI. When fat suppression was used with contrast-enhanced MRI, you could not differentiate definitely between the fat in hilum and the focal defect.

### *CT and MRI for the Diagnosis of Nodal Metastasis in the Neck*

The general consensus is that small, borderline-sized nodes without necrosis are not reliably differentiated from reactive nodes in patients with head and neck cancer (2). Further, it is considered that MRI has little contribution to the diagnostic accuracy of contrast-enhanced CT. Indeed, a comparative study using the ROC analysis for combined information on size and internal abnormality indicated that CT performed slightly better than MRI; the Az values obtained were 0.80 and 0.75 for CT and MRI, respectively (10). The authors of this preceding study also demonstrated that the size criterion of smaller than 10 mm resulted in high negative predictive values at the expense of positive predictive values. The lack of definitive diagnostic methods for metastatic nodes may lead to an elective neck dissection in order to avoid missing small metastatic nodes, because a large number of patients are clinically staged as N0 neck (1,18).

Considering these backgrounds, we would like to postulate that in addition to the nodal size criteria the criteria that are based on the changes in the internal architecture of the node should be assessed for the precise imaging diagnosis of metastatic nodes. In this regard, the internal changes such as liquefaction or coagulation necrosis, cancer nests, and keratin depos-

its, which were previously described as "abnormal signal intensity" on MR images (10), may be important clues to the diagnosis of metastatic nodes.

Recent advances in MRI technology have enabled fast high-resolution MRI by using a coil with a high local sensitivity, thereby greatly improving its diagnostic ability as compared to that of CT (13,19,20). To obtain high-resolution MR images within a short image acquisition time we used surface coils coupled with the SENSE and CLEAR techniques. However, more detailed nodal architecture could be revealed when a smaller-sized surface coil (for example, a 47-mm microscopy coil) is used; the microscopy coil allows the assessment of a small (smaller than 3 mm in diameter) necrotic focus in a metastatic node in the neck (13). Although MR microimaging is time-consuming, suffers from a small FOV, and cannot be applied to deep nodes, it is yet a promising technique to further improve the diagnostic accuracy, for example, in applying to suspicious, borderline nodes.

A recent study using diffusion-weighted MRI indicated that apparent diffusion coefficients (ADCs) may provide additional information that is distinct from morphological features (13,19). ADCs are markers of cell density and can distinguish malignant lesions from benign lesions. The metastatic nodes were found to have significantly higher ADCs than the benign or reactive nodes in the necks of the patients with head and neck squamous cell carcinoma (13). This was mainly due to the presence of liquefaction necrosis in metastatic cancers. Therefore, the impact of using ADCs in diagnosing N0-necks of patients with head and neck cancer still remains to be clarified. However, the functional features of lymph nodes such as ADCs and contrast-enhanced MRI using iron oxide particles (21–23) reflect the biological activity of cancer cells and lymph tissues. Hence, they could be used as promising techniques for the detection of metastatic nodes in the neck in combination with high-resolution MRI.

Multidetector CT (MDCT) permits rapid examination, and it produces higher resolutions and multiplanar reformation of the images. We have not yet tested whether MDCT can offer an improved diagnostic ability to differentiate metastatic nodes from reactive nodes in the neck. Although the diagnostic ability of MDCT to detect metastatic nodes was reported to be relatively lower than that of MRI (24), the diagnostic potential of MDCT in the neck will be clarified in the future studies.

### *MRI Strategy for Diagnosing Metastatic Nodes*

Taken together, we conclude that MRI is superior to CT in the diagnosis of metastatic nodes from head and neck squamous cell carcinomas, particularly for the detection of small, borderline-sized (<10 mm in minimum axis diameter) nodes in the neck. For the optimal lymph node characterization, we recommend contrast-enhanced T1-weighted imaging and fat-suppressed (SPIR) T2-weighted imaging for the detection of focal defects in metastatic nodes. When any definitive focal defect is not detected by the sequences and a node is superficially located, in particular with small-sized nodes, a high-resolution MRI using a small-sized surface coil such as a microscopy coil may be beneficial in detecting metastatic cancer focus with or without nodal necrosis on fat-suppressed T2-weighted images.

The present study cohort included many patients with multiple metastases in the neck. The presence of multiple metastases would significantly influence the planning of radiotherapy, especially in determining the radiation field. Therefore, an effective surveying technique is mandatory. MRI could also be used as a surveying technique for the detection of metastatic nodes in the neck; the turbo short inversion time inversion recovery (STIR) imaging technique was favorably appraised for that purpose (25). The detection of cancer focus is an important clue for the differentiation between metastatic and reactive nodes. In addition to the assessment of nodal architecture, functional MRI, for example, diffusion-weighted imaging, and contrast-enhanced MRI using iron peroxide particles may be supportive for the diagnosis of metastatic nodes. Doppler sonography and sonography-guided fine-needle aspiration cytology could be adjuncts to the cross-sectional imaging techniques (26).

## REFERENCES


1. Layland MK, Sessions DG, Lenox L. The influence of lymph node metastasis in the treatment of squamous cell carcinoma of the oral cavity, oropharynx, larynx and hypopharynx: N0 versus N+. Laryngoscope 2005;115:629–639.
2. Anzai Y, Brunberg JA, Lufkin RB. Imaging of nodal metastases in the head and neck. J Magn Reson Imaging 1997;7:774–783.
3. Silverman PM. Lymph node imaging: multidetector CT (MDCT). Cancer Imaging 2005;5:S57–67.
4. Suojanen JN, Mukherji SK, Dupuy DE, Takahashi JH, Costello P. Spiral CT in evaluation of head and neck lesions: work in progress. Radiology 1992;183:281–283.
5. Korkmaz H, Cerezci NG, Akmansu H, Dursun E. A comparison of spiral and conventional computerized tomography methods in diagnosing various laryngeal lesions. Eur Arch Otorhinolaryngol 1998;255:149–154.
6. Steinkamp HJ, Hosten N, Richter C, Schedel H, Felix R. Enlarged cervical lymph nodes at helical CT. Radiology 1994;191:795–798.
7. Eida S, Sumi M, Koichi Y, Kimura Y, Nakamura T. Combination of helical CT and Doppler sonography in the follow-up of patients with clinical N0 stage neck disease and oral cancer. AJNR Am J Neuroradiol 2003;24:312–318.
8. Sumi M, Ohki M, Nakamura T. Comparison of sonography and CT for differentiating benign from malignant cervical lymph nodes in patients with squamous cell carcinoma of the head and neck. AJR Am J Roentgenol 2001;176:1019–1024.
9. King AD, Tse GMK, Ahuja AT, et al. Necrosis in metastatic neck nodes: diagnostic accuracy of CT, MR imaging, and US. Radiology 2004;230:720–726.
10. Curtin HD, Ishwaran H, Mancuso AA, Dalley RW, Caudry DJ, McNeil BJ. Comparison of CT and MR imaging in staging of neck metastases. Radiology 1998;207:123–130.
11. Don DM, Anzai Y, Lufkin RB, Fu YS, Calcaterra TC. Evaluation of cervical lymph node metastasis in squamous cell carcinoma of the head and neck. Laryngoscope 1995;105:669–674.
12. Chikui T, Yonetsu K, Nakamura T. Multivariate feature analysis of sonographic findings of metastatic cervical lymph nodes: contribution of blood flow features revealed by power Doppler sonography for predicting metastasis. AJNR Am J Neuroradiol 2000;21:561–567.
13. Sumi M, Van Cauteren M, Nakamura T. MR microimaging of benign and malignant nodes in the neck. AJR Am J Roentgenol 2006;186:749–757.
14. Metz CE. ROC methodology in radiologic imaging. Invest Radiol 1986;21:720–733.

15. Hanley JA, McNell BJ. The meaning and use of the area under a receiver operating characteristic (ROC) curve. Radiology 1982;143:29–36.
16. van den Brekel MWM, Stel HV, Castelijns JA, et al. Cervical lymph node metastasis: assessment of radiologic criteria. Radiology 1990; 177:379–384.
17. Nakamura T, Sumi M. Nodal imaging in the neck: recent advances in US, CT and MR imaging of metastatic nodes. Eur Radiol 2007; 17:1235–1241.
18. Pitman KT. Sentinel node localization in head and neck tumors. Semin Nucl Med 2005;35:253–256.
19. Sumi M, Sakihama N, Sumi T, et al. Discrimination of metastatic cervical lymph nodes with diffusion-weighted MR imaging in patients with head and neck cancer. AJNR Am J Neuroraiol 2003;24:1627–1634.
20. King AD, Tse GMK, Yuen EHY, et al. Comparison of CT and MR imaging for the detection of extranodal neoplastic spread in metastatic neck nodes. Eur J Radiol 2004;52:264–270.
21. Anzai Y, Blackwell KE, Hirschowitz SL, et al. Initial clinical experience with dextran-coated superparamagnetic iron oxide for detection of lymph node metastases in patients with head and neck cancer. Radiology 1994;192:709–715.
22. Anzai Y, Prince MR. Iron oxide-enhanced MR lymphography: the evaluation of cervical lymph node metastases in head and neck cancer. J Magn Reson Imaging 1997;7:75–81.
23. Baghi M, Mack MG, Hambek M, et al. The efficacy of MRI with ultrasmall superparamagnetic iron oxide particles (USPIO) in head and neck cancers. Anticancer Res 2005;25:3665–3670.
24. Matsuoka H, Nakamura A, Masaki T, et al. A prospective comparison between multidetector-row computed tomography and magnetic resonance imaging in the preoperative evaluation of rectal carcinoma. Am J Surg 2003;185:556–559.
25. Kawai Y, Sumi M, Nakamura T. Turbo short t inversion recovery imaging for metastatic node screening in patients with head and neck cancer. AJNR Am J Neuroradiol 2006;27:1283–1287.
26. van den Brekel MWM. Lymph node metastases: CT and MRI. Eur J Radiol 2000;33:230–238.